ACS APPLIED ELECTRONIC MATERIALS

Open Access

This article is licensed under CC-BY 4.0

pubs.acs.org/acsaelm

Article

Management of Triplet Electronic Excitations in Derivatives of Phenoxathiin and Benzophenone

Asta Dabuliene,* Mathis Quignon, Oleksandr Bezvikonnyi, Rasa Keruckiene, Mohamed Abdella, Jurate Simokaitiene, Dmytro Volyniuk, and Juozas Vidas Grazulevicius*

Cite This: ACS Appl. Electron. Mater. 2025, 7, 6137−6148

Read Online

ACCESS | Metrics & More | Article Recommendations | Supporting Information

ABSTRACT: A series of donor−acceptor (D−A) compounds consisting of phenoxathiin, phenothiazine, or dimethylacridan electron donating moieties and a benzophenone electron accepting core are designed and synthesized via the Suzuki or Buchwald−Hartwig cross-coupling reaction. By varying the donor units, as well as by introducing heavy bromine atoms into the molecular structure, the impact of nature of the donor moieties on the thermal, electrochemical, and photophysical properties of the benzophenones is studied by theoretical and experimental means. The compounds containing two donor units exhibit higher glass transition temperatures than monosubstituted benzophenones. For molecularly doped polymeric matrices containing 1 wt % of the derivatives with only phenoxathiin units and bromine atoms in their structures, room-temperature phosphorescence is observed. Meanwhile, asymmetric compounds that have phenothiazine or dimethylacridan donor units show thermally activated delayed fluorescence when doped in a polymeric matrix. The polymer molecularly doped with 4-phenoxathiin-4-yl-benzophenone exhibits high sensitivity to oxygen reaching up to 1.8×10^{-3} ppm^{-1}. 4-(9,9-Dimethylacridan-10-yl)-4′-(phenoxathiin-4-yl)benzophenone exhibits high hole and electron drift mobilities of 6.9×10^{-4} $cm^2/(V\ s)$ and 7.8×10^{-4} $cm^2/(V\ s)$, respectively at the electric field of 5.14×10^5 V/cm. It also shows good performance in the emissive layer of the organic light emitting diode characterized by an external quantum efficiency of 17%. This work signifies the importance of the rational design of derivatives of phenoxathiin and benzophenone as emitters for the effective utilization of triplet energy in optical and optoelectronic applications.

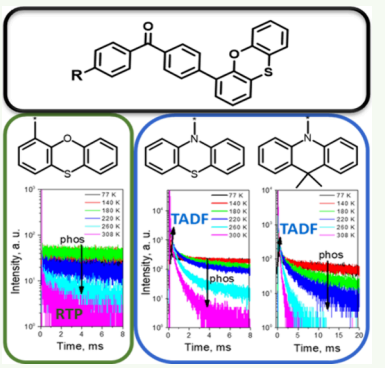

KEYWORDS: *phenoxathiin, benzophenone, triplet exciton, TADF, RTP, oxygen sensing*

Downloaded via 88.222.25.29 on July 9, 2025 at 07:14:05 (UTC).
See https://pubs.acs.org/sharingguidelines for options on how to legitimately share published articles.

1. INTRODUCTION

Tuning of the molecular structures of organic emitters provides unique advantages of the exploitation of triplet excitons in photonics and optoelectronics. In the case of excitation by electricity, holes and electrons injected into thin films of organic semiconductors form degenerate polaron pairs due to Coulomb interactions. Then, the purely statistical probability determines the singlet and triplet states of the pairs. The continuous localization of the polaron pairs results in the formation of singlet and triplet Frenkel excitons in the ratio one 1 to 3 in optoelectronic devices.[1] This distribution of singlet and triplet excitons reflects four possible combinations of the orientation of spin angular momentums of an electron−hole pair. Contrary, the excitons formed by photoexcitation are initially singlet, as the respective states of the electron−hole pairs are systematic and not statistical in nature. Upon optical pumping, the triplet excited states of organic luminophores are populated through intersystem crossing (ISC) from the singlet excited states. The deactivation of triplet electronic excitation in conventional organic luminophores involves a spin-forbidden transition to the singlet ground state, making phosphorescence generally improbable for the emitters at room temperature. Recently, different pathways of the utilization of triplet excited energy in emission were discovered including thermally activated delayed fluorescence (TADF), electrophosphorescence (PhOLEDs), hybridized local charge transfer states, hot exciton mechanism, triplet−triplet annihilation, room temperature phosphorescence (RTP), hyperfluorescence, multiresonant TADF, etc.[2,3] TADF is an emission of triplet excitons upconverted to the singlet excited states via reverse intersystem crossing (RISC) due to molecular motions induced by thermal energy.[3] The phenomenon requires a small difference in energy levels between the first singlet and triplet excited states, which can be achieved for fully organic emitters. Consequently, TADF is an ecofriendly approach for the fabrication of OLEDs in contrast to electrophosphorescence. The small singlet−triplet energy splitting requires minimal overlap of wave functions of the molecular orbitals involved in the emissive process.[3] It can be

Received: April 28, 2025
Revised: June 11, 2025
Accepted: June 11, 2025
Published: June 20, 2025

© 2025 The Authors. Published by American Chemical Society

achieved by managing exciplexes and designing donor−acceptor structures.[4] The alternative path to employ triplet excitons in emission is to enhance spin−orbit interactions in fully organic emitters without using noble metal complexes.[5,6] Insertion of S and Br atoms into the structures of emitters is often considered as a useful approach for the realization of RTP.[6] A classic way to obtain an efficient RTP is to achieve efficient ISC which is reached through spin−orbit coupling (SOC).[7] As more structure−property relationships were examined, cases of the appearance of both TADF and RTP in the same emitters were reported.[8,9] The different triplet-facilitated phenomena can be activated in the same types of materials under varying conditions. Consequently, the different spectral manifestations of the phenomena open pathways for advanced multifunctional applications of the emitters in optical sensing, bioimaging devices, and organic light-emitting diodes (OLEDs).[10−13] As the employment of triplet excitons in emission allows substantially increasing the efficiency of the OLEDs, the quenching of triplet energy can be useful for sensing applications.

Organic emitters exhibiting RTP as oxygen sensing probes were reported recently.[14−16] Oxygen is essential for virtually all living organisms. It played a pivotal role in evolutionary processes. Consequently, oxygen sensing is of significant importance in various fields, including biology and medicine.[17,18] The applications of oxygen sensors range from noninvasive health monitoring[19] and food and pharmaceutical packaging[20,21] to the control of industrial processes and environmental monitoring.[22] Within this context, oxygen sensing represents one of the most important application domains in RTP materials. Optical oxygen sensors are widely utilized in food technology and packaging, medicine, biotechnology, environmental sciences, and geosciences.[6,22] Nevertheless, most of the reported RTP oxygen analytes have several drawbacks, such as environmental sensitivity and low emission efficiency.[23,24] Such limitations highlight the need for further research on stable and efficient RTP materials. The study of the effect of the molecular structure on triplet emission mechanisms remains of great interest. To achieve efficient TADF or RTP under ambient conditions, it is crucial to suppress the vibrational and oxygen-mediated quenching of triplet excitons. Molecular design plays a pivotal role in minimization of these quenching processes.

Here, we report on a series of derivatives of phenoxathiin and benzophenone (PB). The electron-withdrawing benzophenone moiety is widely used in the design of the structures of organic emitters intended for OLEDs.[25−28] The phenoxathiin moiety is still scarcely used as an electron-donating unit. It is expected that an atom of S could enhance the ISC and SOC processes to ensure efficient RTP.[29] The synthesized compounds are characterized by a high thermal stability. Inspired by the above-discussed developments in exploitations of triplet energy in a variety of applications, the derivatives of phenoxathiin and benzophenone were designed, aiming at the management of triplet excited states. The incorporation of the strong electron-donating phenothiazine and dimetylacridan moieties resulted in enhanced intramolecular charge transfer (CT) and the consequent switching from RTP to TADF.[30−32] The Stern−Volmer constants for the oxygen sensitivity of TADF and RTP of the synthesized emitters were found to be $0.9-1.8 \times 10^{-3}$ ppm^{-1} which are comparable to the state-of-the-art values. The derivative of dimethylacridan exhibits an efficient TADF. OLED with this emitter shows an external quantum efficiency (EQE) of 17%. Most importantly, triplet electronic excitations were utilized in both optical and electronic applications based on the different emissive processes. The structure−property relationships were established for the derivatives of phenoxathiin and PB revealing the principles of utilization of triplet excitons in different applications.

2. EXPERIMENTAL SECTION

2.1. Instrumentation. A Bruker Avance III [400 MHz (^{1}H), 101 MHz (^{13}C)] apparatus was used for recording ^{1}H NMR and ^{13}C NMR spectra at room temperature. Chemical shifts (δ) are reported in ppm referenced to tetramethylsilane or to the internal solvent signal. Mass spectra (MS) were recorded on a Waters ZQ (Waters, Milford, MA). IR spectra were recorded by a Vertex 70 Bruker spectrometer equipped with an ATR attachment with a diamond crystal over frequencies of 600−3500 cm^{-1} with a resolution of 5 cm^{-1} over 32 scans. An Avantes AvaSpec-2048XL spectrometer was used for the recording of absorption spectra. An Edinburgh Instruments FLS980 spectrometer was used for measurements of emission spectra and decay curves. A Sepia II PicoQuant laser with an excitation wavelength of 374 nm was used for the measurements of photoluminescence decay curves. An Optistat DN2 cryostat and a turbomolecular pump were used for recording emission spectra and decay curves at different temperatures in the deoxygenated environment.

A gas-flow controller SmartTrak 50 and mass flow meter SmartTrak 100 were used for the estimation of the sensitivity of emission to oxygen at room temperature and at the relative humidity of 0%. A chamber with a sample holder was filled with a mixture of oxygen and nitrogen gases for the measurements.

Kurt J. Lesker equipment built in the MBRAUN EcoVap4G glovebox was used for the preparation of samples and fabrication of OLEDs by thermal vacuum evaporation technique under high vacuum (2×10^{-6} mbar). The rate of deposition was in the range of 1−2 Å/s. OLEDs were fabricated without passivation. A Keithley 2400C sourcemeter, PH100-Si-HA-D0 calibrated photodiode, and PC-based power and energy monitor 11S-LINK were used for the simultaneous measurements of the current density−voltage and luminance−voltage characteristics of the OLEDs. The time-resolved electroluminescence (TREL) measurements were performed with a 10 V bias at 5 kHz with a 50% duty cycle.

Differential scanning calorimetry (DSC) measurements were carried out using a DSC Q 2000. Thermogravimetric analysis (TGA) was performed on a TGA Q 50. The TGA and DSC curves were recorded in a nitrogen atmosphere at a heating rate of 10 °C/min. The cyclic voltammetry (CV) measurements were carried out by a three-electrode assembly cell from Bio-Logic SAS and a micro-AUTOLAB Type III potentiostat−galvanostat apparatus. The working electrode was a glassy carbon with a surface of 0.12 cm^2. The reference electrode and the counter electrode were Ag/Ag^+ 0.01 M and Pt wire, respectively. The solutions with the concentration of 10^{-3} M of the compounds in argon-purged dichloromethane (Fluka) with tetrabulthylammonium perchlorate (TBAP; 0.1 M) as the electrolyte were used for the CV measurements. Charge mobilities were studied by the time-of-flight (TOF) method. The transient current curves were collected by applying different positive or negative voltages using a 6517B electrometer (Keithley) to the optically transparent electrode (ITO) to monitor the transport of holes or electrons, respectively. A TDS 3032C oscilloscope (Tektronix) was used for recording of the photocurrent transients of holes or electrons. The hole and electron transit times (t_{tr}) were obtained at different electric fields. The values of t_{tr} were used for the calculation of hole (μ_h) and electron (μ_e) flights at various electric fields using the formula $\mu_{h/e} = d^2/(U \cdot t_{tr})$, where t_{tr} is the transit time, d is the thickness of a layer, and U is the applied voltage. The thickness of a layer (d) was estimated using an optical profilometer (Profilm3D). The TOF mobility values as the

https://doi.org/10.1021/acsaelm.5c00863
ACS Appl. Electron. Mater. 2025, 7, 6137−6148

Scheme 1. Synthesis of PB Derivatives

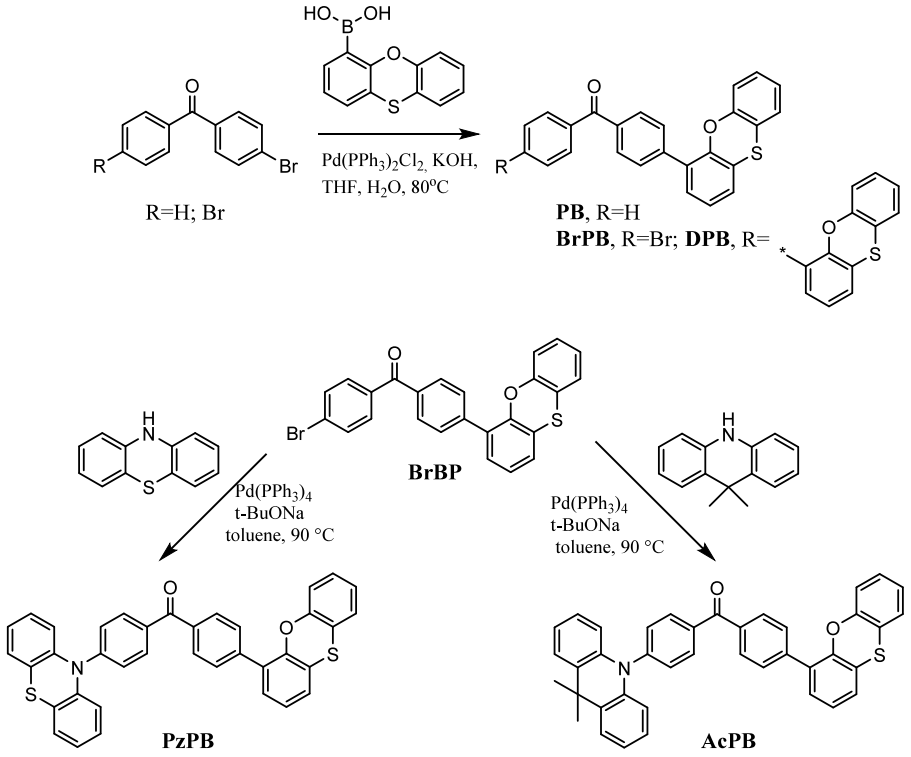

function of electric fields (E) were well-fitted using the Poole−Frenkel formula $\mu = \mu_0 \exp \beta E^{1/2}$.

Melting points of the compounds were estimated by an electrothermal melt-temp 1101D (Dubuque, IA, USA) apparatus (error value ± 1 °C). Theoretical calculations were carried out using Gaussian 16 and Gaussview 6 software.

2.2. Materials. Phenoxathiin-4-yl boronic acid, 4-bromobenzophenone, 4,4-dibromobenzophenone, 9,9-dimethyl-9,10-dihydroacridine, and phenothiazine were purchased from Sigma-Aldrich and Fluorochem and used as received. Zeonex in the study denotes Zeonex 480 donated by Zeon Europe GmbH.

2.3. Synthesis and Identification. NMR spectra of the compounds are presented in the SI.

*4-Phenoxathiin-4-yl-benzophenone (**PB**).* A dried 100 mL flask was charged with phenoxathiin-4-yl boronic acid (0.5 g, 2 mmol), 4-bromobenzophenone (0.68 g, 2.6 mmol), bis(triphenylphosphine)-palladium(II) dichloride ($Pd(PPh_3)_2Cl_2$) (0.07g, 0.1 mmol), and powdered potassium hydroxide (1.12 g, 20.00 mmol). The reaction vessel was vacuumed and filled with argon. Degassed tetrahydrofuran (THF) (30 mL) and degassed water (5 mL) were added, and the reaction mixture was stirred at 80 °C for 3 h. The crude product was extracted into DCM, and the organic phase was washed with water and dried over Na_2SO_4. The product was purified by column chromatography using hexane/ethyl acetate (8/1) as the eluent and recrystallized from the eluent. The yield of white crystals (mp = 156−157 °C) was of 74%.

^{1}H NMR (400 MHz, $CDCl_3$), δ (ppm): 7.94 (d, J = 8.1 Hz, 2H), 7.89 (d, J = 7.5 Hz, 2H), 7.67 (d, J = 8.1 Hz, 2H), 7.63−7.60 (m, 1 H), 7.52 (t, J = 7.5 Hz, 1H), 7.22 (d, J = 7.9 Hz, 1H), 7.18−7.08 (m, 4H), 7.03(t, J = 7.4 Hz, 1H), 6.92 (d, J = 7.9 Hz, 1H).

^{13}C NMR (100 MHz, $CDCl_3$), δ (ppm): 196.42, 152.47, 149.30, 141.50, 137.74, 136.46, 132.48, 13009, 130.05, 129.53, 128.40, 127.89, 126.93, 126.89, 124.94, 124.59, 122.08, 120.98, 117.72.

$C_{25}H_{16}O_2S$ [$(M+H)^+$] exact mass = 381.09, MS ($APCI^+$) = 381.00.

*4-Bromo-4′-phenoxathiin-4-yl-benzophenone (**BrPB**).* **BrPB** was synthesized by the same method as MQ7 from phenoxathiin-4-yl boronic acid (0.5 g, 2 mmol), 4,4-dibromobenzophenone (1.05 g, 3,1 mmol), $Pd(PPh_3)_2Cl_2$ (0.07 g, 0.1 mmol), KOH (1.15 g, 20.5 mmol), 30 mL of THF, and 5 mL of water. The yield of white crystals (mp = 140−141 °C) was of 61%.

^{1}H NMR (400 MHz, $CDCl_3$), δ (ppm): 7.90 (d, J = 8.1 Hz, 2H), 7.76 (d, J = 8.3 Hz, 2H), 7.69−7.67 (m, 4H), 7.24−7.11 (m, 5H), 7.05 (t, J = 7,4 Hz, 1H), 6.91 (d, J = 7.9 Hz, 1H).

^{13}C NMR (100 MHz, $CDCl_3$), δ (ppm): 195.35, 152.45, 149.29, 141.80, 136.45, 136.03, 131.70, 131.57, 129.90, 129.63, 129.14, 127.87, 126.99, 126.89, 124.94, 124.57, 122.11, 120.95, 117.68.

$C_{25}H_{15}BrO_2S$ [M^+] exact mass = 458.00, MS (ESI^+) = 458.03.

*4,4′-Diphenoxathiin-4-yl-benzophenone (**DPB**).* **DPB** was synthesized by the same method as MQ7 from phenoxathiin-4-yl boronic acid (0.5 g, 4 mmol), 4,4-dibromobenzophenone (0.7 g, 2 mmol), $Pd(PPh_3)_2Cl_2$ (0.14 g, 0.2 mmol), KOH (1.15 g, 20.5 mmol), 30 mL of THF, and 5 mL of water. The yield of white crystals (mp = 146−148 °C) was of 67%.

^{1}H NMR (400 MHz, $CDCl_3$), δ (ppm): 8.00 (d, J = 8.3 Hz, 4H), 7.71 (d, J = *8,3 Hz, 4H),* 7.25−7,27 (m, 2H), 7.12−7.21 (m, 8 H), 7.03−7.07 (m, 2H), 6.92−6.95 (m, 2H).

^{13}C NMR (100 MHz, $CDCl_3$), δ (ppm): 196.19, 152.51, 149.33 141.52, 136.58, 130.58, 130.0, 129.57, 129.19, 127.87, 126.92, 126.89, 124.92, 124.57, 122.10, 120.99, 117.73.

$C_{37}H_{22}O_3S_2$ [M^+] exact mass = 578.10, MS (ESI^+) = 578.14.

*4-(9,9-Dimethylacridan-10-yl)-4′-(phenoxathiin-4-yl)-benzophenone (**AcPB**).* A dried 100 mL flask was charged with 9,9-dimethyl-9,10-dihydroacridine (0.118 g, 0.57 mmol), 4-bromo-4′-phenoxathiin-4-yl-benzophenone (MQ2) (0.2 g, 0.44 mmol), *t*-BuONa (0.251g, 2.61 mmol), $Pd(PPh_3)_4$ (0.03 g, 0.03 mmol), and dry toluene (5 mL). The reaction mixture was heated at 100 °C for 3 h. After cooling down, the reaction mixture was diluted with DCM, and the organic phase was washed with water and brine. After being dried over Na_2SO_4 and filtered, the solvent was removed, and the residue was purified by column chromatography using hexane/toluene (2:1) as the eluent and recrystallized from the eluent mixture of solvents. The yield of yellowish crystals (mp = 176−177 °C) was of 81%.

^{1}H NMR (400 MHz, $CDCl_3$), δ (ppm) 8.15 (d, J = 8.0 Hz, 2H), 8.03 (d, J = 7.9 Hz, 2H), 7.73 (d, J = 7.9 Hz, 2H), 7.48−7.53(m, 4H),

https://doi.org/10.1021/acsaelm.5c00863
ACS Appl. Electron. Mater. 2025, 7, 6137−6148

7.21 (s, 1H), 7.12−7.21 (m, 4H), 6.93−7.07 (m, 6H), 6.37(d, J = 8.0 Hz, 2H), 1.71(s, 6H).

^{13}C NMR (100 MHz, $CDCl_3$), δ (ppm): 207.0, 195.5, 152.46, 149.31, 145.42, 141.82, 140.50, 137.13, 136.17, 132.69, 130.98, 130.64, 130.46, 130.02, 129.67, 129.18, 127.88, 126.99, 126.44, 125.37, 124.94, 124.59, 122.11, 121.12, 120.94, 117.71, 114.37, 30.94.

$C_{40}H_{29}NO_2S$ [$(M+H)^+$] exact mass = 588.19, MS (US^+) = 588.03.

*4-(Phenothiazin-10-yl)-4′-(phenoxathiin-4-yl)benzophenone (**PzPB**).* **PzPB** was synthesized by the same method as MQ4 from phenothiazine (0.17g, 0.85 mmol) and 4-bromo-4′-phenoxathiin-4-yl-benzophenone (0.30g, 0.66 mmol), t-BuONa (0.38 g, 3.94 mmol), $Pd(PPh_3)_4$ (0.06 g, 0.05 mmol), and dry toluene (5 mL). The yield of brownish crystals (mp = 241−242 °C) was of 58%.

^{1}H NMR (400 MHz, THF), δ (ppm): 7.91 (d, J = 7.9 Hz, 2H), 7.71 (d, J = 8.1 Hz, 2H), 7.33 (d, J = 8.5 Hz, 2H), 7.30−7.12 (m, 9H), 7.07−7.02 (m, 3H), 6.97−6.92 (m, 3H).

^{13}C NMR (100 MHz, THF), δ (ppm): 194.06, 153.38, 150.11, 147.92, 143.44; 141.75, 137.68, 134.55, 132.73, 131.50, 130.32, 130.06, 129.94, 128.59, 128.47, 128.43, 127.81, 127.46, 125.62, 125.34, 125.23, 123.07, 122.83, 122.58, 121.78; 118.31.

$C_{37}H_{23}NO_2S_2$ [M^+] exact mass = 577.12, MS (ESI^+) = 577.36.

3. RESULTS AND DISCUSSION

Synthesis, Thermal, and Electrochemical Properties. The donor−acceptor (D−A) compounds consisting of electron acceptor benzophenone and electron donor phenoxathiine (**PB**, **BrPB**, and **DPB**) were synthesized by Suzuki cross-coupling reactions of phenoxathiin-4-yl boronic acid with monobromo or dibromo derivatives of benzophenone in the presence of catalytic amounts of $Pd(PPh_3)_2Cl_2$ in the mixture of THF and H_2O (Scheme 1). The asymmetric D−A−D′ type molecules were synthesized by the Buchwald−Hartwig cross-coupling reaction of 4-bromo-4′-phenoxathiin-4-yl-benzophenone (**BrBP**) with electron-donating phenothiazine or dimethylacridan with the yield of the product of 58−81% (Scheme 1).

The thermal transitions and thermal stability of PB derivatives were studied by differential scanning calorimetry (DSC) and thermogravimetric analysis (TGA) under a nitrogen atmosphere. The data are given in Table 1. The compounds were isolated after synthesis as crystalline substances. The first DSC scans of the synthesized PB derivatives revealed melting points (T_m) in the range of 143−246 °C. After slow cooling the second heating scans revealed for all compounds the signals of glass transition at 28−87 °C (Figure 1a). Neither melting nor crystallization signals were observed during these scans (Figure S11). The values of 5% weight loss temperatures (T_d) of PB derivatives were in the range of 314−390 °C as confirmed by TGA (Table 1, Figure 1b). Single-stage TG curves up to complete weight loss of compounds **PB**, **BrPB**, and **DPB** show that 5% weight loss temperatures correspond to the temperatures of the onsets of sublimation of these compounds.

Table 1. Thermal, Electrochemical, and Photoelectrical Characteristics of PB Derivatives

Compound[a]	PB	BrPB	DPB	AcPB	PzPB
T_g, °C[b]	28	40	79	82	87
T_m, °C[c]	160	143	172	181	246
$T_{-5\%}$, °C	317	315	416	387	391
$E^{ox}_{onset\ vs\ Fc}$, V	0.72	0.75	0.77	0.49	0.29
$E^{red}_{onset\ vs\ Fc}$, V	−2.15	−2.01	−2.06	−2.03	−2.04
E_{EA}, eV	2.65	2.79	2.74	2.77	2.76
E_i, eV	5.52	5.55	5.57	5.29	5.09

[a]$T_{-5\%}$ − 5% mass loss temperature determined by TGA, heating rate of 20 °C/min, N_2 atmosphere. T_g − glass transition temperature, T_m − melting point, determined by DSC, scan rate of 10 °C/min, N_2 atmosphere. [b]Second heating scan. [c]First heating scan.

Cyclic voltammetry (CV) measurements were conducted for the estimation of the electrochemical characteristics of the PB derivatives. All the studied compounds exhibited reversible oxidation upon multiple scans (Figure S12). The CV curves of PB derivatives maintained consistent shapes throughout successive cycles, indicating the formation of stable radical cations and radical anions. The ionization energy (E_i) values were estimated based on the oxidation onset potentials relative to ferrocene (E_{ox} onset versus Fc). The E_i values for the PB derivatives ranged from 5.09 to 5.57 eV (Table 1). The presence of the second phenoxathiine group did not influence the E_i value. This was observed by comparing the E_i of **DPB** with those of **PB** and **BrPB**. The replacement of phenoxathiin fragment by either dimethylacridan or phenothiazine moieties resulted in the decrease of E_i by 0.28 and 0.48 eV, respectively (cf. E_i of **DPB** with **AcPB** or **PzPB**). The electron affinity (E_{EA}) values derived from the CV of the PB derivatives were found to be in the close range from 2.65 to 2.79 eV. These E_{EA} values were calculated using the E_i values and the reduction potential onsets with respect to ferrocene.

Excited States. In order to obtain the optimized geometry, the frontier molecular orbital distributions, and energy levels of the compounds, density functional theory (DFT) calculations at the B3LYP/6-31^{+2}G theoretical level in vacuum were performed (Figure 2).

The derivatives of benzophenone-substituted phenoxathiin and phenothiazine possess a relatively planar molecular conformation, characterized by a dihedral angle between the donor and acceptor units of ca. 50°. This structural arrangement leads to significant separation of the highest occupied molecular orbitals (HOMOs) and the lowest unoccupied molecular orbitals (LUMOs). Although phenoxathiin and phenothiazine serve as electron-donating units, their molecular cores deviate from planarity due to the heavy atom effect, which significantly influences the electronic structure and conjugation pathways[33,34] The nonplanar core of the donor moieties translates into a slight extension of the LUMO from the acceptor moiety toward the donor moieties. The HOMOs are delocalized on the slightly bent phenoxathiin and phenothiazine moieties. The HOMO of compound **AcPB** is delocalized on the planar dimethylacridan moiety. This unique spatial and electronic configuration ultimately modulates the absorption and emission characteristics of these derivatives, as discussed in further chapters. The theoretically obtained HOMO values are in agreement with the experimental results. The most shallow HOMO was observed for compound **AcPB** having the strongest electron donor, i.e., dimethylacridine moiety (Figure 2).

The absorption spectra of toluene and tetrahydrofuran (THF) solutions of the PB derivatives were recorded at room temperature (Figure 3a). The absorption spectra of THF solutions have one intense band at ca. 300 nm. The absorption spectrum of the THF solution of **PzPB** has a CT band peaking at 339 nm. Except for the CT band of **PzPB**, all the absorption bands of the solutions of the studied compounds undergo insignificant shifts in their location when the polar THF is replaced with a nonpolar toluene highlighting their locally excited (LE) character (Figure 3a, Figure S13).

https://doi.org/10.1021/acsaelm.5c00863
ACS Appl. Electron. Mater. 2025, 7, 6137−6148

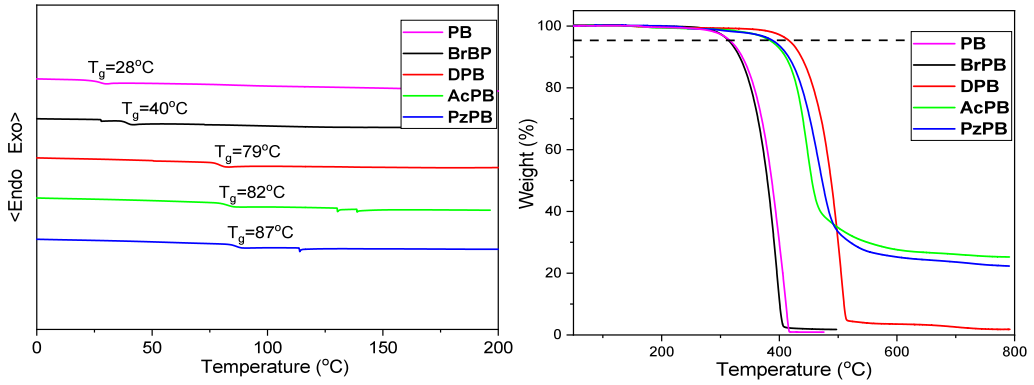

Figure 1. DSC curves (the second heating scans) of phenoxathiin-based compounds recorded at the heating rate of 10 °C min^{-1} in nitrogen atmosphere (a). TGA curves of phenoxathiin derivatives recorded at the heating rate of 20 °C min^{-1} in the nitrogen atmosphere (b).

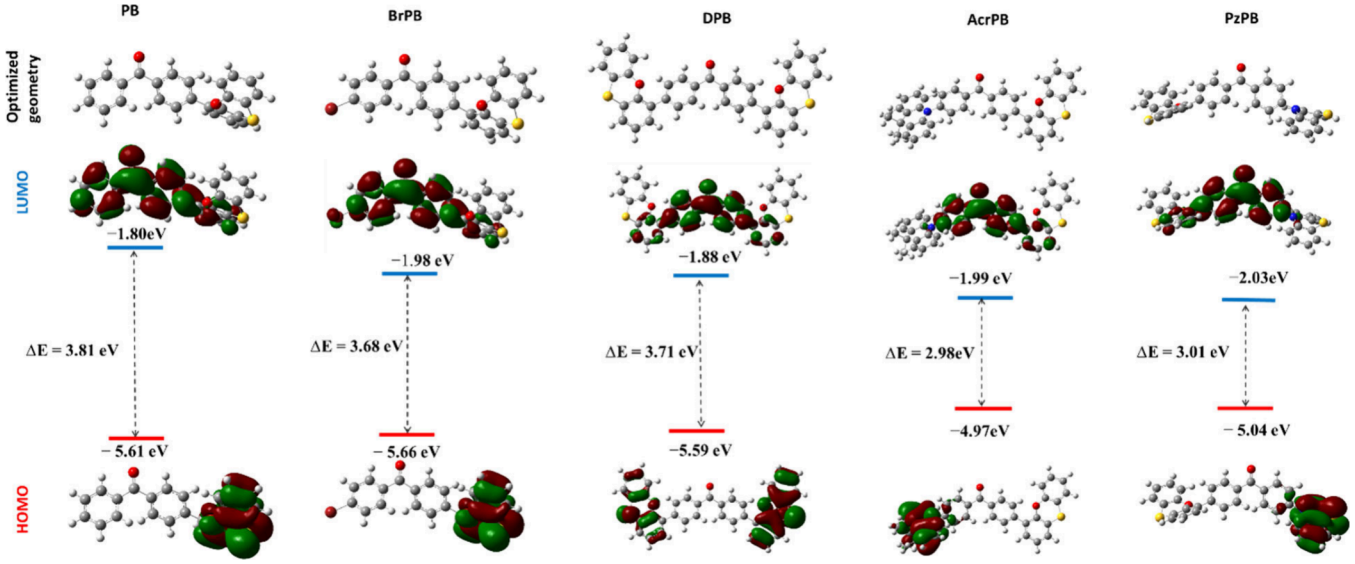

Figure 2. Molecular orbital distribution of the compounds at the ground state level (calculated in vacuum).

Molar absorption coefficients of the solutions of **AcPB** and **PzPB** which have stronger donor moieties than phenoxathiin are increased when toluene is replaced by more polar THF (Figure S13). The only exclusion is the n−π^* absorption peak for PzPB attributed to phenothiazine, having practically identical coefficient values when the polarity of the solvent is changed. The toluene solutions of **BrPB**, **DPB**, and **PB** containing only phenoxathiin units, and the Br atom in the structure of **BrPB**, exhibit higher molar absorption coefficients than the corresponding THF solutions. This observation indicates the distinctive difference in the optical properties of the two subgroups of compounds in the series.

TD-DFT (B3LYP/6-31 + G **) calculations allow deeper insights into the nature of the experimental absorption bands. The theoretical UV spectra of the compounds are very similar to those of their toluene and THF solutions (Figure S14), exhibiting a strong band located in the higher energy range. The UV absorption bands of the theoretical spectra of the compounds are characterized by transitions toward several excited states but are dominated by $S_0 \rightarrow S_3$ transitions for compounds **DP** and **BrDP**. The dominating transition of the derivative of the disubstituted benzophenone (**DPB**) is the $S_0 \rightarrow S_4$ transition. Whereas the theoretical UV spectra of **AcPB** and **PzPB** are dominated by the transitions to higher excited states ($S_0 \rightarrow S_6$, $S_0 \rightarrow S_8$, respectively). Nevertheless, these transitions represent mixtures of local acceptor excitations (LE) and acceptor-to-donor CT excitations (Figure S14a−d). The excited state of the lowest-energy S_1 corresponds to the HOMO→LUMO transition with negligible oscillator strengths (f) of 0.000. These theoretical results suggest that the lowest energy transitions $S_0 \rightarrow S_1$ do not contribute significantly to the absorption spectra of the benzophenone derivatives studied. Both the experimental and the theoretical results thus indicate that the optical properties of these benzophenone derivatives are determined by the intramolecular transitions in solutions.

The emission bands of the solutions of the compounds are bathochromically shifted with the increase of polarity of the solvent by 30−55 nm, manifesting the intramolecular CT state of the emission (Figure 3a). The positions of the bands of photoluminescence (PL) spectra are determined by the nature of the donor moieties. Thus, the solutions of **BrPB** and **PB** consisting of only benzophenone and phenoxathiin moieties exhibit almost identical PL spectra with a negligible PL quantum yield (PLQY). However, the addition of the second phenoxathiin donor unit to the structure of the compound (**DPB**) resulted in a red shift of the PL peak location from 454 to 459 nm due to the extension of π-conjugation. Dimethylacridan is a strong electron donor, causing the shift

https://doi.org/10.1021/acsaelm.5c00863
ACS Appl. Electron. Mater. 2025, 7, 6137−6148

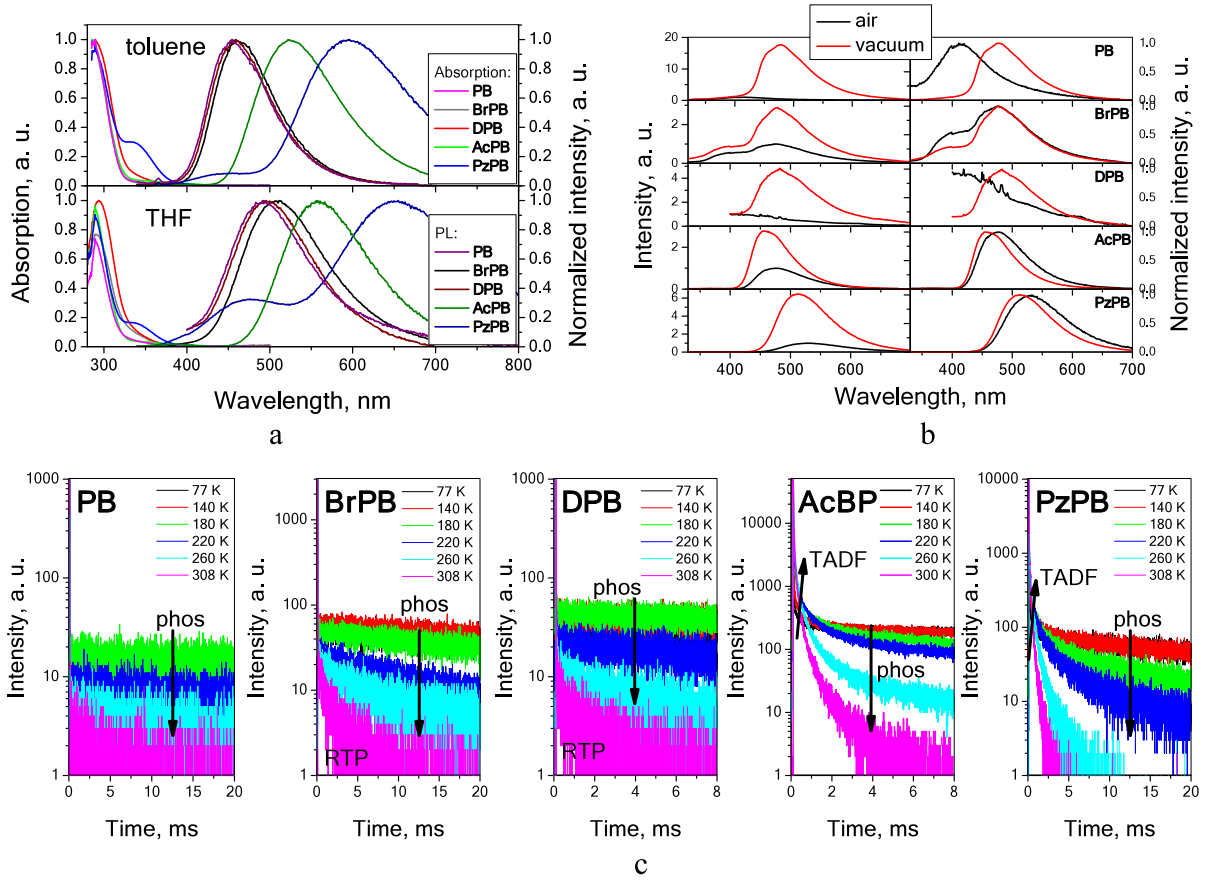

Figure 3. Absorption and PL spectra of dilute toluene and THF solutions of the compounds recorded at room temperature (a). Non-normalized and normalized PL spectra of the films of the compounds doped in Zeonex 480 (1 wt %) recorded at room temperature (b). PL decay curves of the films of the compounds doped in Zeonex 480 (1 wt %) recorded at the peak wavelengths at different temperatures (c).

of the PL peak of the solution of **AcPB** to the yellowish-green spectral range and the increase of PLQY of the deoxygenated toluene solution to 13.5%. The main peak of the PL spectra of the toluene solution of **PzPB** containing phenothiazine moiety is red-shifted further to 595 nm with a PLQY value of 1.7%. The PL band of the THF solution peaks at 653 nm. The occurrence of two CT peaks for the phenothiazine-containing donor−acceptor compound **PzPB** was reported before assigning the blue PL peak to the *q-ax* conformers and the orange/red PL peak to the *q-eq* conformers of phenothiazine moiety.[35]

In order to further investigate the photophysical properties and to minimize the intermolecular interactions, which could potentially result in quenching of the emission, the compounds were molecularly dispersed in the rigid Zeonex 480 polymer matrix. The increase of PL intensity was observed for all the films after evacuation (Figure 3b). In the PL spectra of the films of the molecular dispersions of **PB**, **BrPb**, and **DPB** in Zeonex 480, the low-energy bands with a distinctive vibronic structure appeared at ca. 477 nm. In addition, the increase of intensity of PL bands was observed after evacuation. For the molecular mixture of **PB** and Zeonex, an increase of PL intensity by a factor of 17.7 was observed. The bands observed in PL spectra at 477 nm corresponded to those of the phosphorescence spectra recorded at 77 K (Figure S15). The lifetimes of emission were in the microsecond range (Table S1, Figure 3c, Figures S16−S20). The differences of intensities of the PL bands recorded in air-equilibrated and oxygen-free environments indicate the involvement of triplets in the emission of benzophenone derivatives containing a phenoxathiine moiety. Since PL intensity is sensitive to the presence of oxygen, it is suggested that the origin of emission is RTP. The polymer molecularly doped with benzophenone derivatives **AcPB** and **PzPB** containing the stronger electron donating moieties, i.e., dimethylacridan and phenothiazine, exhibited 2.8 and 6.5-fold increases of PL intensity after the evacuation of the solid samples (Figure 3b). This observation also indicates an active radiative recombination from the triplet state. The singlet−triplet energy splitting values of 0.02 eV observed for **AcPB** and 0.01 eV for **PzPB** indicate that the origin of emission was delayed fluorescence. For further confirmation of the delayed fluorescence, temperature-dependent PL measurements were performed. Normalized PL spectra (Figure S21) and PL decay curves (Figure 3c, Figure S22) of the films of **BrPB**, **DPB**, and **PB** doped in Zeonex matrix, exhibited the gradual phosphorescence quenching with the increase of temperature and the change of the relative distribution of intensity of the bands of prompt fluorescence and phosphoresce. The films of **AcPB** and **PzPB** doped in Zeonex exhibited a consecutive decrease in the phosphorescence and an increase in DF upon the increase in the temperature. Hence, the thermal activation of DF is postulated from the dynamics of PL decay curves of the films of the dimethylacridan (**AcPB**)- and phenothiazine (**PzPB**)-based emitters recorded at different temperatures (Figure 3c).

https://doi.org/10.1021/acsaelm.5c00863
ACS Appl. Electron. Mater. 2025, 7, 6137−6148

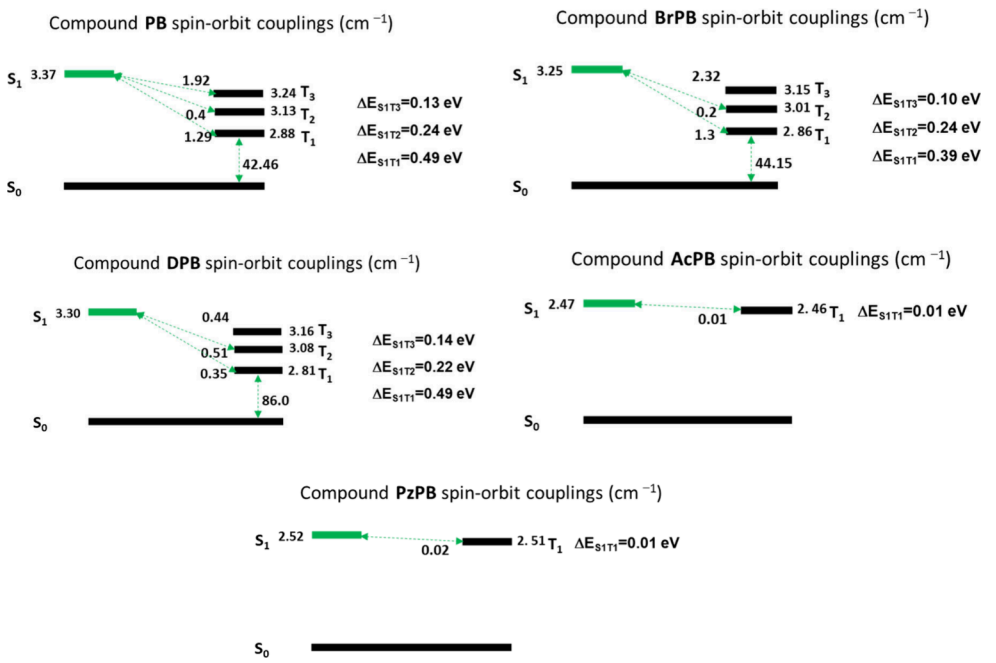

Figure 4. Calculated SOC values and excited state energy levels of the **PB** derivatives.

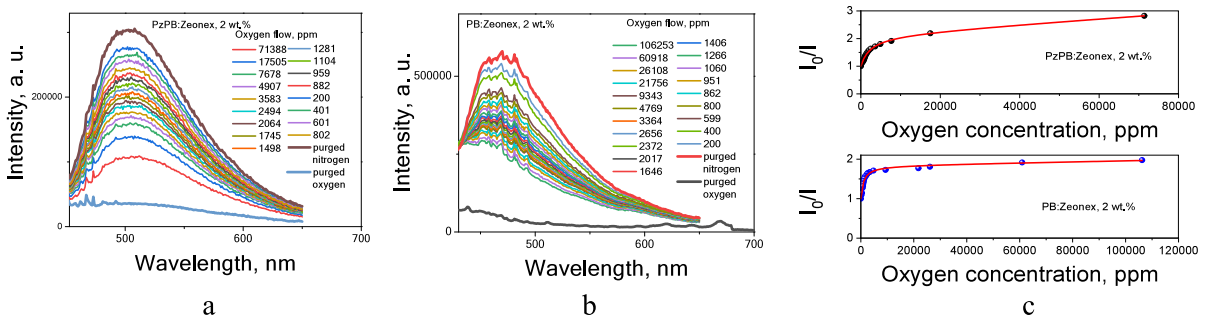

Figure 5. PL spectra of the films of **PzPB** (a) and **PB** (b) doped in Zoenex (2 wt %) recorded at the different oxygen concentrations. The Stern–Volmer plots of the films (c).

The theoretical calculations help to delve into the electronic structure of the benzophenone derivatives and provide additional information about their emission properties. The results indicate that the S_1 excited states of the series of compounds studied exhibit a distinct CT character (Figure S23). Meanwhile, T_1 is localized and associated with the benzophenone moiety, indicating an LE nature. Taking into account the excited states energy diagram, RTP exhibiting compounds **PB**, **BrPB**, and **DPB** have three triplet energy states below S_1 (Figure 4). The relatively high SOC values support efficient intersystem crossing (ISC) by facilitating transitions to the three lower-lying triplet states. In contrast, the TADF active compounds **AcPB** and **PzPB** display minimal energy gaps between their S_1 and T_1 states. This near-degeneracy results in low SOC values, significantly promoting RISC and thereby enhancing TADF efficiency. Such distinctions in SOC values and configurations of excited states arise from D–A systems of benzophenone derivatives and determine their emissive properties.

Notably, the nonplanar geometry of phenoxathiin reduces its electron-donating capability, potentially hindering CT interactions. This leads to the enhancement of SOC and ISC, hence enhancing the dominance of the benzophenone acceptor, making these systems more favorable for RTP. In contrast, stronger and more planar electron-donating units such as dimethylacridan improve charge separation, reduce singlet–triplet energy gap, and accelerate RISC, optimizing these compounds for efficient TADF.

Practical Applications of Triplet-Facilitated Phenomena Exhibited by PB Derivatives. Taking into account the considerable emission response of the compounds to the collisional interactions with oxygen and the biggest increase of PL intensity after the deoxygenation, the concentration-dependent oxygen sensing tests were performed using the films of **PzPB** and **PB** doped in Zeonex (2 wt %) (Figure 5c). The samples were placed in an isolated chamber with a controlled atmosphere. The PL spectra of the films were recorded under nitrogen and subsequently under a controlled increasing concentration of oxygen with a 5 min interval. The tests were finished with measurements under an oxygen atmosphere (Figure 5a,b).

The PL spectra totally corresponded to the above-discussed PL spectra of the compounds, highlighting the TADF of **PzPB** and RTP of **PB** (Figure 3b). The intensity of emission decreases upon increasing oxygen concentration in the chamber. The nature of emission quenching is an interception of triplet energy.[36] It is discussed in more detail in SI. The ratios of emission intensity observed at the peak wavelength

https://doi.org/10.1021/acsaelm.5c00863
ACS Appl. Electron. Mater. 2025, 7, 6137–6148

Table 2. Data Derived from Stern–Volmer Plots of Films of PzPB and PB Doped in Zeonex

Sample	f_1	k_{SV1}, ppm^{-1}	f_2	k_{SV2}, ppm^{-1}	LOD, ppm	*Adj.* R^2
PB:Zeonex (2 wt %)	0.54	8.8×10^{-4}	0.46	4.6×10^{-6}	3.4, 652.2	0.996
PzPB:Zeonex (2 wt %)	0.54	6.9×10^{-7}	0.46	1.8×10^{-3}	1.6, 4375	0.974

Table 3. Major Characteristics of OLEDs[a]

OLED	Doping, wt %	Current efficiency, cd/A	Power efficiency, lm/W	EQE, %	λ, nm	1931 CIE$_{x,y}$	J_0, mA/cm^2	τ_{1-3}, μs	τ_{avg}, μs	χ^2
A	1	34.9/26.1	15.9/7.5	14.7/10.9	488	(0.19, 0.36)	16.1	6.2, 22.3, 109.4	46.3	1.049
B	1	38.7/29.4	21.4/8.6	15.4/11.7	488	(0.19, 0.38)	24	7.2, 24.8, 115.2	55.1	1.097
C	10	42.1/41.6	14.1/13.6	15.8/15.6	497	(0.18, 0.44)	69.4	6.2, 21.9, 106.8	39.2	1.091
D	10	41.6/40.2	14.0/13.0	15.7/15.2	501	(0.18, 0.45)	62.3	6.3, 22.1, 107.2	43.6	1.075
E	15	43.8/40.3	19.0/13.3	15.6/14.3	504	(0.20, 0.48)	67.9	6.4, 22.3, 102.2	33.2	1.096
F	15	48.2/42.0	19.4/11.7	17.0/14.8	504	(0.20, 0.49)	ca. 53	8.0, 25.2, 103.4	37.3	1.053

[a]Efficiency values are presented as maximum values/values at 1000 cd/m^2.

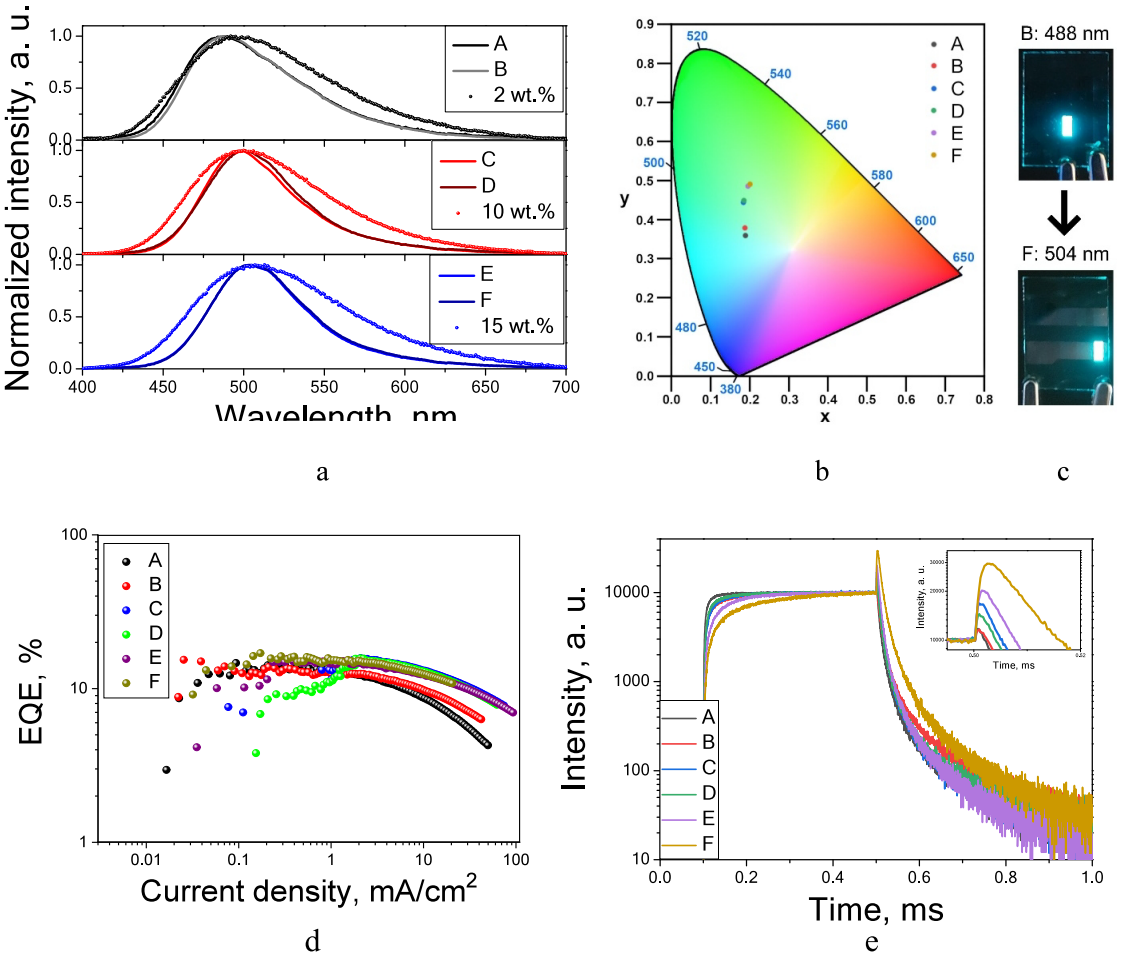

Figure 6. EL spectra of OLEDs and PL spectra of the films of **AcPB** doped in mCP (2, 10, and 15 wt %) (a). 1931 CIE diagram of the OLEDs (b). Photos of mCP-based OLEDs B and F (c). EQE–current density plots of the OLEDs (d). TREL profiles of OLEDs (e).

under nitrogen (I_0) and of the emission intensity recorded at the specific oxygen concentration (I) were taken for the estimation of the Stern–Volmer constants k_{SV}. The dependence between I_0/I and the oxygen concentration $[O_2]$ exhibited a downward curvature. Therefore, the Stern–Volmer equation for quasi-hyperbolic correlation which describes two independent spectroscopic responses with fractions f_1 and f_2 was used: $\frac{I_0}{I} = \left[\frac{f_1}{1+k_{SV1}[O_2]} + \frac{f_2}{1+k_{SV2}[O_2]}\right]^{-1}$.[37] The fits of the plots represent two components of the optical sensitivity to the oxygen with the precision of *adj.* R^2 of >0.99 and 0.97 for the samples of the polymer molecularly doped with **PzPB** and **PB**, respectively. The data obtained are collected in Table 2.

The nonexponential and nonlinear Stern–Volmer response is assigned to the inhomogeneity due to spatial disorder in the film of the molecularly doped Zeonex and the diffusion effects. The rigidity of the polymeric host apparently results in the limited interaction of the molecules of the guests with

https://doi.org/10.1021/acsaelm.5c00863
ACS Appl. Electron. Mater. 2025, 7, 6137–6148

oxygen.[38] The values of f_1 and f_2 were found to be close for both the samples, highlighting the identical procedure of the film fabrication and ultimately the very same reason for two components of the optical sensitivity to oxygen. The PB-based sample with the k_{SV} of 1.8×10^{-3} and the limit of detection of 1.6 ppm is comparable with the corresponding values recently reported for RTP oxygen sensing analytes.[22,39,40]

Unlike RTP, TADF can be used effectively in optoelectronics. TADF emitter **AcPB** was tested in the emissive layers of OLEDs. The structures of the devices were as follows: ITO/HAT-CN/TCTA/mCP/the emitting layer of **AcPB** doped into host matrix/TSPO1/TPBi/LiF/Al. The thickness of the layers and the dopant concentration within the emitting layer were changed in order to optimize the devices and enhance the triplet-facilitated emission of the **PB** derivative in the most effective way. Detailed information about the structures of the OLEDs is given in the SI. The main characteristics of the OLEDs are collected in Table 3, Figure 6, and Figures S24−S30. 1,4,5,8,9,11-Hexaazatriphenylenehexacarbonitrile (HAT-CN) and LiF were selected for hole and electron injection, respectively. Tris(4-carbazoyl-9-ylphenyl)amine (TCTA) and 2,2′,2″-(1,3,5-Benzinetriyl)-tris(1-phenyl-1-H-benzimidazole) (TPBi) were employed for the deposition of hole and electron transporting layers, respectively. 1,3-Bis(N-carbazolyl)benzene (mCP) and diphenyl[4-(triphenylsilyl)phenyl]phosphine oxide (TSPO1) were chosen for the fabrication of electron and hole blocking layers, respectively. The EL spectra of OLEDs A−F remain stable upon increasing voltage and correspond to the emission spectrum of the film of **AcPB** manifesting complete electronic excitation energy transfer from host to guest (Figure 6a, Figures S24a−S29a). The color of electroluminescence in the 1931 CIE coordinates shifted from sky blue to green with the increase of concentration of **AcPB** from 1 to 15 wt % in the emitting layer (Figure 6b, c). The EL spectra of the OLEDs totally correspond to the PL spectra of the films with the respective concentrations (Figure 6a). The PL spectra are broader than the corresponding EL spectra due to enhanced intermolecular interactions caused by the thickness of the films being higher than 25−28 nm of the emitting layers of the OLEDs.

Devices A and B were fabricated with the concentration of **AcPB** of 1 wt %. 3,3′-Di(9H-carbazol-9-yl)-1,1′-biphenyl (mCBP) was taken as a host for OLED A and mCP was selected as a host for device B. Both devices exhibited similar EL spectra with peaks at 488 nm. As the mCP-based OLED exhibited slightly higher efficiency than that of the OLED A, mCP was used in the further optimization of the device structure. The concentration of **AcPB** was increased to 10 wt % in devices C and D. The thicknesses of the layers of TCTA and mCP were increased from 31 to 40 nm and from 4 to 6 nm in OLEDs C and D, respectively. The changes in the thickness did not have any significant effect on the efficiency or the turn-on voltage. This observation shows that the limits of the OLED performance are reached not because of the charge balance issues related to the charge transporting layers but rather because of the emissive species themselves. There was a minor change in emission characteristics as the peak of EL spectra shifted from 497 to 500 nm after the increase of the concentration of the emitter in the host (Figure 6a). The increase of the concentration of **AcPB** from 1 to 10 wt % resulted in the reduction of turn-on voltage to ca. 4.4 V and the increase of EQE to 15.8%. The efficiency roll-off was also improved to values close to the maximum one at 1000 cd/m^2 (Table 3, Figure 6d). The critical current density j_0 is defined as the current density at which the EQE is half of its maximum value. The values j_0 are used as a measure of the efficiency roll-off. They are listed in Table 3. To understand the reason behind the improved performance, transient EL (TREL) signals of the OLEDs were recorded (Figure 6e). The triple exponential fits were applied to the TREL profiles. The lifetimes of the components (τ_{1-3}) are given in Table 3. The initial rise of the TREL edge is associated with the initial recombination of excitons in the recombination zone and trapping, detrapping, and recombination of charge carriers.[41] As the bias is switched off, the injected carriers drift back to the respective electrodes under an internal electric field. The back-propagating charges corresponding to the excitons that are trapped cause a TREL overshoot. The overshoot originates from the recombination of electron−hole pairs and unpaired charges that undergo trapping. With the increase of the dopant concentration in the emitting layer, the overshoot becomes more intensive, linking **AcPB** directly with the trap formation. TREL also indicates the trend of the decrease of the EL lifetime of the longest-lived component τ_3 as well as of the decrease of the average lifetime τ_{avg} upon increasing concentration of **AcPB** in the host. Shortening of the TADF lifetime enhances the RISC rate and improves the resistance of OLEDs to the efficiency roll-off.[42] Thus, the increase of **AcPB** concentration in the host from 1 to 10 wt % resulted in more efficient TADF. The further increase from 10 wt % for C and D to 15 wt % for E and F led to a further decrease of the TADF lifetime. However, the distinction in terms of the efficiency of OLEDs with the concentrations of the emitter of 15 wt % and 10 wt % was minor. The difference between the structure of the OLEDs E and F with 15 wt % concentration of **AcPB** was the thickness of the layer of LiF. The decrease in the thickness of the layer of LiF from 0.8 nm for E to 0.5 nm resulted in the decrease of the operating voltage by 1 V and the increase of the maximum EQE from 15.6 to 17%. This observation can be explained by the improved charge balance. Although the maximum value of EQE of the OLED F reached 17%, the EQEs of devices E and F observed at the current densities higher than 1 mA/cm^2 were lower than the corresponding values of the OLEDs C and D (Figure 6d). The increase of the dopant concentration from 10 to 15 wt % resulted in the increased efficiency roll-off indicated by the reduced j_0. As TADF is the emissive mechanism of the OLEDs, overpopulation of triplet states facilitated phenomena such as triplet−triplet annihilation, triplet-polaron quenching, etc., considered as the primary reasons for efficiency roll-off.[43] Devices E and F with the higher concentration of the emitter in the emitting layer expectedly exhibited larger TREL overshoots, highlighting more massive trap formation that additionally contributed to the efficiency roll-off. The positions of the EL peak further shifted to 504 nm with the increase of the concentration of **AcPB** from 10 to 15 wt %. The preferable concentration of the emitter was 10 wt %. It allowed the higher efficiency of the device to be reached at higher luminance. Taking into account the relatively high τ_{avg}, it can be argued that the roll-off is remarkably small for the fabricated OLEDs exhibiting TADF. This observation can be explained by the fact that the **AcPB** is characterized by bipolar charge transport. The charge drift mobility values of 6.9×10^{-4} and 7.8×10^{-4} cm^2/(V s) for holes and electrons, respectively, were obtained for **AcPB** using the TOF technique at an electric field of 5.14×10^5 V/cm (Figure S31a). Such mobility values rank among the

https://doi.org/10.1021/acsaelm.5c00863
ACS Appl. Electron. Mater. 2025, 7, 6137−6148

best for organic semiconductors used in OLEDs.[44] The balance of efficient hole and electron transport in the wide range of electric fields suggests the efficient recombination of hole−electron pairs. The character of transient current curves (Figure S31b,c) indicates the dispersive transport of charge carriers leading to the broadening of the recombination zone of excitons in the OLEDs based on **AcPB** and the consequent decrease of the efficiency roll-off.[45] The device efficiency comparable with that of the previously reported OLED based on dimethylacridan disubstituted benzophenone derivative (DMAC-BP; EQE = 18.9%) makes **AcPB** a promising TADF emitter for further investigation.[26]

CONCLUSIONS

The study highlights the tunable emissive properties of donor−acceptor compounds consisting of phenoxathiin, phenothiazine, or dimethylacridan donor moieties and benzophenone acceptor units. It is experimentally and theoretically demonstrated that the nonplanar phenoxathiin moiety facilitates room-temperature phosphorescence due to its reduced electron-donating capacity, especially when paired with benzophenone and heavy bromine atoms. The emission of 4-phenoxathiin-4-yl-benzophenone demonstrates exceptional oxygen sensitivity, reaching up to 1.8×10^{-3} ppm^{-1}. This makes the compound highly suitable for optical oxygen-sensing applications. Incorporation of the stronger, planar donor moieties such as dimethylacridan results in the shift of the emission mechanism to TADF, optimizing spatial charge separation and reversed intersystem crossing. OLEDs containing 4-(9,9-dimethylacridan-10-yl)-4′-(phenoxathiin-4-yl)-benzophenone exhibited external quantum efficiency of up to 17%. The emitter had the highest efficiency when its concentration in the emitting layer was 10 wt %. At this concentration, the TADF enhancement combined with minimal trap formation resulted in the reduction of the efficiency roll-off over the wide luminance range. The color of the electroluminescence can be tuned from sky blue to green by tuning the dopant concentration with rather small changes in the efficiency of the devices. These findings underscore the critical role of donor−acceptor pairing, heavy-atom effects, and structural tuning in the optimization of thermal, electrochemical, and photophysical properties of derivatives phenoxathiin and benzophenone for the rational use of triplet electronic excitations in oxygen sensing and efficient OLEDs.

ASSOCIATED CONTENT

Supporting Information

The Supporting Information is available free of charge at https://pubs.acs.org/doi/10.1021/acsaelm.5c00863.

^{1}H and ^{13}C NMR spectra of synthesized materials **PB**, **BrPB**, **DPB**, **AcPB**, and **PzPB**. DSC graphs of PB derivatives. Cyclic voltammograms of PB compounds. Additional photophysical data including absorption spectra of PB materials in dilute toluene, and THF solutions, PL and phosphorescence spectra of films of PB compounds doped in Zeonex 480 (1 wt %) at 77 K, and theoretical UV spectra of PB compounds and their dominating transitions. PL decay curves of films of **PB**, **BrPB**, **DPB**, **AcPb**, and **PzPB** doped in Zeonex 480 (1 wt %) at room temperature. PL decay curves of the film of **PB** doped in Zeonex 480 (1 wt %) at 77 and 308 K. Theoretically calculated S1 and T1 natural transition orbitals of PB derivatives. Triplet quenching by oxygen. The structure and thickness of the layers of the fabricated OLEDs. EL spectra, correlation of current density and brightness vs voltage, correlation of current and power efficiency, EQE vs current density of devices A−F and TREL profiles of OLEDs A−F. TOF measurements. TOF mobility values of the film of**AcPB** as a function of electric fields at room temperature. TOF signals of the film of **AcPB** recorded under positive and negative voltages at ITO. (PDF)

AUTHOR INFORMATION

Corresponding Authors

Juozas Vidas Grazulevicius − *Department of Polymer Chemistry and Technology, Faculty of Chemical Technology, Kaunas University of Technology, LT-51423 Kaunas, Lithuania;* orcid.org/0000-0002-4408-9727; Email: juozas.grazulevicius@ktu.lt

Asta Dabuliene − *Department of Polymer Chemistry and Technology, Faculty of Chemical Technology, Kaunas University of Technology, LT-51423 Kaunas, Lithuania;* Email: asta.dabuliene@ktu.lt

Authors

Mathis Quignon − *University of Artois - Béthune IUT, 62400 Béthune Cedex, France;* orcid.org/0009-0001-7500-9427

Oleksandr Bezvikonnyi − *Department of Polymer Chemistry and Technology, Faculty of Chemical Technology, Kaunas University of Technology, LT-51423 Kaunas, Lithuania; KTU "M-Lab" Laboratory Center, Kaunas University of Technology, LT-51369 Kaunas, Lithuania*

Rasa Keruckiene − *Department of Polymer Chemistry and Technology, Faculty of Chemical Technology, Kaunas University of Technology, LT-51423 Kaunas, Lithuania;* orcid.org/0000-0002-9809-5815

Mohamed Abdella − *Department of Polymer Chemistry and Technology, Faculty of Chemical Technology, Kaunas University of Technology, LT-51423 Kaunas, Lithuania;* orcid.org/0009-0007-5672-9211

Jurate Simokaitiene − *Department of Polymer Chemistry and Technology, Faculty of Chemical Technology, Kaunas University of Technology, LT-51423 Kaunas, Lithuania*

Dmytro Volyniuk − *Department of Polymer Chemistry and Technology, Faculty of Chemical Technology, Kaunas University of Technology, LT-51423 Kaunas, Lithuania*

Complete contact information is available at: https://pubs.acs.org/10.1021/acsaelm.5c00863

Author Contributions

The manuscript was written through contributions of all authors. All authors have given approval to the final version of the manuscript.

Notes

The authors declare no competing financial interest.

ACKNOWLEDGMENTS

This project has received funding from the Research Council of Lithuania (LMTLT), agreement No. S-MIP-23-50.

REFERENCES

(1) Forrest, S. R. Exciton Formation Statistics under Electrical Injection in Organic Semiconductor Thin Films. *J. Lumin.* **2004**, *110* (4), 378−383.

(2) Dos Santos, J. M.; Hall, D.; Basumatary, B.; Bryden, M.; Chen, D.; Choudhary, P.; Comerford, T.; Crovini, E.; Danos, A.; De, J.; Diesing, S.; Fatahi, M.; Griffin, M.; Gupta, A. K.; Hafeez, H.; Hämmerling, L.; Hanover, E.; Haug, J.; Heil, T.; Karthik, D.; Kumar, S.; Lee, O.; Li, H.; Lucas, F.; Mackenzie, C. F. R.; Mariko, A.; Matulaitis, T.; Millward, F.; Olivier, Y.; Qi, Q.; Samuel, I. D. W.; Sharma, N.; Si, C.; Spierling, L.; Sudhakar, P.; Sun, D.; Tankelevičiūtė, E.; Duarte Tonet, M.; Wang, J.; Wang, T.; Wu, S.; Xu, Y.; Zhang, L.; Zysman-Colman, E. The Golden Age of Thermally Activated Delayed Fluorescence Materials: Design and Exploitation. *Chem. Rev.* **2024**, *124* (24), 13736−14110.

(3) Tankelevičiūtė, E.; Samuel, I. D. W.; Zysman-Colman, E. The Blue Problem: OLED Stability and Degradation Mechanisms. *J. Phys. Chem. Lett.* **2024**, *15* (4), 1034−1047.

(4) Chapran, M.; Pander, P.; Vasylieva, M.; Wiosna-Salyga, G.; Ulanski, J.; Dias, F. B.; Data, P. Realizing 20% External Quantum Efficiency in Electroluminescence with Efficient Thermally Activated Delayed Fluorescence from an Exciplex. *ACS Appl. Mater. Interfaces* **2019**, *11* (14), 13460−13471.

(5) Patil, Y.; Demangeat, C.; Favereau, L. Recent Advances in Room Temperature Phosphorescence of Chiral Organic Materials. *Chirality* **2023**, *35* (7), 390−410.

(6) Ji, M.; Ma, X. Recent Progress with the Application of Organic Room-Temperature Phosphorescent Materials. *Industrial Chemistry & Materials* **2023**, *1* (4), 582−594.

(7) Leitonas, K.; Tomkeviciene, A.; Baratte, G.; Dabuliene, A.; Punniyakoti, S. M.; Volyniuk, D.; Grazulevicius, J. V. Oxygen Sensing Properties of Thianthrene and Phenothiazine Derivatives Exhibiting Room Temperature Phosphorescence: Effect of Substitution of Phenothiazine Moieties. *Sens Actuators B Chem.* **2021**, *345*, No. 130369.

(8) Hosono, T.; Decarli, N. O.; Crocomo, P. Z.; Goya, T.; de Sousa, L. E.; Tohnai, N.; Minakata, S.; de Silva, P.; Data, P.; Takeda, Y. The Regioisomeric Effect on the Excited-State Fate Leading to Room-Temperature Phosphorescence or Thermally Activated Delayed Fluorescence in a Dibenzophenazine-Cored Donor−Acceptor−Donor System. *J. Mater. Chem. C Mater.* **2022**, *10* (12), 4905−4913.

(9) Klimash, A.; Prlj, A.; Yufit, D. S.; Mallick, A.; Curchod, B. F. E.; McGonigal, P. R.; Skabara, P. J.; Etherington, M. K. From Phosphorescence to Delayed Fluorescence in One Step: Tuning Photophysical Properties by Quaternisation of an Sp2-Hybridised Nitrogen Atom. *J. Mater. Chem. C Mater.* **2022**, *10* (25), 9484−9491.

(10) Mahaan, R.; Panneerselvam, M.; Costa, L. T.; Bosco, A. J. Unveiling the Influence of Oxidation State and Heavy Atom Effects in Chalcogen Group on Boron Centered D(X)BNA Core: A Computational Study on RTP versus TADF. *Mol. Syst. Des Eng.* **2025**, *10*, 102.

(11) Mahaan, R.; John Bosco, A. Sulfur Oxidation State and Substituents Influenced Multifunctional Organic Luminophores in BTP Core for OLEDs: A Computational Study on RTP, TADF Emitter and Sensitizer. *J. Phys. Chem. A* **2023**, *127* (50), 10570−10582.

(12) Song, T.; Liu, H.; Ren, J.; Wang, Z. Achieving TADF and RTP with Stimulus-Responsiveness and Tunability from Phenothiazine-Based Donor−Acceptor Molecules. *Adv. Opt Mater.* **2024**, *12* (1), No. 2301215.

(13) Ji, J.; Perepichka, I. F.; Bai, J.; Hu, D.; Xu, X.; Liu, M.; Wang, T.; Zhao, C.; Meng, H.; Huang, W. Three-Phase Electric Power Driven Electroluminescent Devices. *Nature Communications 2021 12:1* **2021**, *12* (1), 1−11.

(14) Wang, Y.; Sun, Z.; Peng, L.; Kou, M.; Qin, F.; Zhang, Z. A Wide Range Oxygen Sensing Strategy with the Collaboration of Multiple Phosphorescence Probes. *Phys. Scr.* **2024**, *99* (7), No. 075038.

(15) Cheng, Z.; Wang, X.; Zhao, J.; Wang, S.; Wu, X.; Tong, H.; Wang, L. Efficient Purely Organic Room-Temperature Phosphorescence from Selenium-Containing Conjugated Polymers for Signal-Amplified Oxygen Detection. *Macromolecules* **2023**, *56* (8), 2972−2979.

(16) Zhao, J.; Wang, X.; Liu, Y.; Cheng, Z.; Wu, X.; Tong, H.; Wang, L. Selenoxanthen-9-One-Based Emitters Exhibiting Efficient Room Temperature Phosphorescence for Electroluminescent and Oxygen Sensing Applications. *Dyes Pigm.* **2024**, *222*, No. 111842.

(17) Shi, H.; Ma, X.; Zhao, Q.; Liu, B.; Qu, Q.; An, Z.; Zhao, Y.; Huang, W. Ultrasmall Phosphorescent Polymer Dots for Ratiometric Oxygen Sensing and Photodynamic Cancer Therapy. *Adv. Funct Mater.* **2014**, *24* (30), 4823−4830.

(18) Papkovsky, D. B.; Dmitriev, R. I. Biological Detection by Optical Oxygen Sensing. *Chem. Soc. Rev.* **2013**, *42* (22), 8700−8732.

(19) Lim, C. J.; Park, J. W. Wearable Transcutaneous Oxygen Sensor for Health Monitoring. *Sens Actuators A Phys.* **2019**, *298*, No. 111607.

(20) Hempel, A.; O'Sullivan, M. G.; Papkovsky, D. B.; Kerry, J. P. Nondestructive and Continuous Monitoring of Oxygen Levels in Modified Atmosphere Packaged Ready-to-Eat Mixed Salad Products Using Optical Oxygen Sensors, and Its Effects on Sensory and Microbiological Counts during Storage. *J. Food Sci.* **2013**, *78* (7), S1057.

(21) Kelly, C. A.; Cruz-Romero, M.; Kerry, J. P.; Papkovsky, D. B. Stability and Safety Assessment of Phosphorescent Oxygen Sensors for Use in Food Packaging Applications. *Chemosensors 2018, Vol. 6, Page 38* **2018**, *6* (3), 38.

(22) Wang, X. D.; Wolfbeis, O. S. Optical Methods for Sensing and Imaging Oxygen: Materials, Spectroscopies and Applications. *Chem. Soc. Rev.* **2014**, *43* (10), 3666−3761.

(23) Zhang, Y.; Sun, Q.; Yue, L.; Wang, Y.; Cui, S.; Zhang, H.; Xue, S.; Yang, W. Room Temperature Phosphorescent (RTP) Thermoplastic Elastomers with Dual and Variable RTP Emission, Photo-Patterning Memory Effect, and Dynamic Deformation RTP Response. *Advanced Science* **2022**, *9* (5), No. 2103402.

(24) Zhan, G.; Liu, Z.; Bian, Z.; Huang, C. Recent Advances in Organic Light-Emitting Diodes Based on Pure Organic Room Temperature Phosphorescence Materials. *Front Chem.* **2019**, *7* (MAY), No. 451835.

(25) Huang, Z.; Yang, D.; Ma, D.; Bin, Z.; You, J. Heptagonal Intramolecular-Lock Strategy Enables High-Performance Thermally Activated Delayed Fluorescence Emitters. *Sci. China Chem.* **2024**, *67* (4), 1181−1186.

(26) Sachnik, O.; Ie, Y.; Ando, N.; Tan, X.; Blom, P. W. M.; Wetzelaer, G. A. H. Single-Layer Organic Light-Emitting Diode with Trap-Free Host Beats Power Efficiency and Lifetime of Multilayer Devices. *Adv. Mater.* **2024**, *36* (16), 2311892.

(27) Zhang, D.; Zhao, C.; Zhang, Y.; Song, X.; Wei, P.; Cai, M.; Duan, L. Highly Efficient Full-Color Thermally Activated Delayed Fluorescent Organic Light-Emitting Diodes: Extremely Low Efficiency Roll-Off Utilizing a Host with Small Singlet−Triplet Splitting. *ACS Appl. Mater. Interfaces* **2017**, *9* (5), 4769−4777.

(28) Zhang, Q.; Tsang, D.; Kuwabara, H.; Hatae, Y.; Li, B.; Takahashi, T.; Lee, S. Y.; Yasuda, T.; Adachi, C. Nearly 100% Internal Quantum Efficiency in Undoped Electroluminescent Devices Employing Pure Organic Emitters. *Adv. Mater.* **2015**, *27* (12), 2096−2100.

(29) Ma, H.; Fu, L.; Yao, X.; Jiang, X.; Lv, K.; Ma, Q.; Shi, H.; An, Z.; Huang, W. Boosting Organic Phosphorescence in Adaptive Host-Guest Materials by Hyperconjugation. *Nat. Commun.* **2024**, *15* (1), 3660.

(30) Qiu, X.; Shi, J.; Xu, X.; Lu, Y.; Sun, Q.; Xue, S.; Yang, W. Tuning the Optoelectronic Properties of Phenothiazine-Based D−A-Type Emitters through Changing Acceptor Pattern. *Dyes Pigm.* **2017**, *147*, 6−15.

(31) Wang, S.; Li, L.; Li, K.; Zhang, T.; Zhao, Z.; Xue, P. Mechanochromism of a Dumbbell D−π−A−π−D Phenothiazine Derivative. *New J. Chem.* **2019**, *43* (33), 12957−12962.

(32) Keruckiene, R.; Guzauskas, M.; Narbutaitis, E.; Tsiko, U.; Volyniuk, D.; Lee, P. H.; Chen, C. H.; Chiu, T. L.; Lin, C. F.; Lee, J. H.; Grazulevicius, J. V. Exciplex-Forming Derivatives of 2,7-Di-Tert-

https://doi.org/10.1021/acsaelm.5c00863
ACS Appl. Electron. Mater. 2025, 7, 6137−6148

Butyl-9,9-Dimethylacridan and Benzotrifluoride for Efficient OLEDs. *Org. Electron* **2020**, *78*, No. 105576.
(33) Banerjee, M.; Anoop, A. Exploring the Theoretical Foundations of Thermally Activated Delayed Fluorescence (TADF) Emission: A Comprehensive TD-DFT Study on Phenothiazine Systems. *Chemistry − A European Journal* **2024**, *30* (20), e202304206.
(34) Liu, H.; Liu, Y.; Chen, G.; Meng, Y.; Peng, H.; Miao, J.; Yang, C. Nonplanar Structure Accelerates Reverse Intersystem Crossing of TADF Emitters: Nearly 40% EQE and Relieved Efficiency Roll Off. *Chem. Sci.* **2024**, *15* (31), 12598−12605.
(35) Sych, G.; Pashazadeh, R.; Danyliv, Y.; Bezvikonnyi, O.; Volyniuk, D.; Lazauskas, A.; Grazulevicius, J. V. Reversibly Switchable Phase-Dependent Emission of Quinoline and Phenothiazine Derivatives towards Applications in Optical Sensing and Information Multicoding. *Chemistry − A European Journal* **2021**, *27* (8), 2826−2836.
(36) Smith, P. O.; Black, D. J.; Pal, R.; Avó, J.; Dias, F. B.; Linthwaite, V. L.; Cann, M. J.; Pålsson, L. O. Applying TADF Emitters in Bioimaging and Sensing—A Novel Approach Using Liposomes for Encapsulation and Cellular Uptake. *Front Chem.* **2021**, *9*, No. 743928.
(37) Berberan-Santos, M. N. Multifunctional Luminescent Platforms for Dual-Sensing. *RSC Nanoscience and Nanotechnology* **2015**, No. 38, 493−507.
(38) Hartmann, P.; Leiner, M. J. P.; Lippitsch, M. E. Luminescence Quenching Behavior of an Oxygen Sensor Based on a Ru(II) Complex Dissolved in Polystyrene. *Anal. Chem.* **1995**, *67* (1), 88−93.
(39) Paisley, N. R.; Tonge, C. M.; Hudson, Z. M. Stimuli-Responsive Thermally Activated Delayed Fluorescence in Polymer Nanoparticles and Thin Films: Applications in Chemical Sensing and Imaging. *Front Chem.* **2020**, *8*, No. 531043.
(40) Armagan, E.; Wei, K.; Fortunato, G.; Amstad, E.; Rossi, R. M. Reversible and Broad-Range Oxygen Sensing Based on Purely Organic Long-Lived Photoemitters. *ACS Appl. Polym. Mater.* **2021**, *3* (5), 2480−2488.
(41) Ghorai, A.; Behera, S. S.; Purohit, S.; Narayan, K. S. Probing Charge Carrier and Triplet Dynamics in TADF-Based OLEDs Using Transient Electroluminescence Studies. *Appl. Phys. Lett.* **2023**, *122* (20), No. 203301.
(42) Serevičius, T.; Skaisgiris, R.; Dodonova, J.; Jagintavičius, L.; Banevičius, D.; Kazlauskas, K.; Tumkevičius, S.; Juršėnas, S. Achieving Submicrosecond Thermally Activated Delayed Fluorescence Lifetime and Highly Efficient Electroluminescence by Fine-Tuning of the Phenoxazine-Pyrimidine Structure. *ACS Appl. Mater. Interfaces* **2020**, *12* (9), 10727−10736.
(43) Jouaiti, A.; Huang, D. C.; Giuso, V.; Cebrián, C.; Mercandelli, P.; Wang, K. H.; Chang, C. H.; Mauro, M. True- to Sky-Blue Emitters Bearing the Thiazolo[5,4- d]Thiazole Electron Acceptor for Single and Tandem Organic Light-Emitting Diodes. *ACS Appl. Electron Mater.* **2023**, *5* (5), 2781−2792.
(44) Mondal, A.; Paterson, L.; Cho, J.; Lin, K.-H.; van der Zee, B.; Wetzelaer, G.-J. A. H.; Stankevych, A.; Vakhnin, A.; Kim, J.-J.; Kadashchuk, A.; Blom, P. W. M.; May, F.; Andrienko, D. Molecular Library of OLED Host Materials—Evaluating the Multiscale Simulation Workflow. *Chemical Physics Reviews* **2021**, *2* (3), 31304.
(45) Murawski, C.; Leo, K.; Gather, M. C. Efficiency Roll-Off in Organic Light-Emitting Diodes. *Adv. Mater.* **2013**, *25* (47), 6801−6827.

https://doi.org/10.1021/acsaelm.5c00863
ACS Appl. Electron. Mater. 2025, 7, 6137−6148